REGULAR ARTICLE

Computational study on the reaction of $CH_3SCH_2CH_3$ with OH radical: mechanism and enthalpy of formation

Jia Cao · Wenliang Wang · Yue Zhang ·
Weina Wang · Tianlei Zhang · Jian Lv ·
Chunying Li

Abstract The reaction mechanism of $CH_3SCH_2CH_3$ with OH radical is studied at the CCSD(T)/6-311+G(3df,p)// MP2/6-31+G(2d,p) level of theory. Three hydrogen abstraction channels, one substitution process and five addition–elimination channels are identified in the title reaction. The result shows hydrogen abstraction is dominant. Substitution process and addition–elimination reactions may be negligible because of the high barrier heights. Enthalpies of formation $[\Delta_f H^o_{(298.15K)}]$ of the reactants and products are evaluated at the CBS-QB3, G3 and G3MP2 levels of theory, respectively. It is found that the calculated enthalpies of formation by the aforementioned three methods are in consistent with the available experimental data. Rate constants and branching ratios are estimated by means of the conventional transition state theory with the Wigner tunneling correction over the temperature range of 200–900 K. The calculation shows that the formations of P1 ($CH_2SCH_2CH_3 + H_2O$) and P2 ($CH_3SCHCH_3 + H_2O$) are major products during 200–900 K. The three-parameter expressio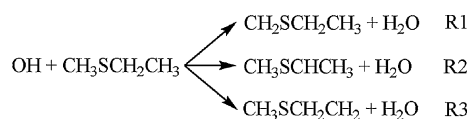ns for the total rate constant is fitted to be $k_{total} =$ $1.45 \times 10^{-21} T^{3.24} \exp(-1384.54/T)$ cm^3 molecule^{-1} s^{-1} from 200 to 900 K.

Keywords $CH_3SCH_2CH_3$ · OH · Mechanism · Enthalpy of formation · Rate constant

J. Cao · W. Wang (✉) · Y. Zhang (✉) · W. Wang · T. Zhang
School of Chemistry and Materials Science,
Shaanxi Normal University, Xi'an, 710062,
People's Republic of China
e-mail: wlwang@snnu.edu.cn

Y. Zhang
e-mail: zhangyue_david@hotmail.com

J. Lv · C. Li
Xi'an Modern Chemistry Research Institute,
Xi'an 710065, People's Republic of China

1 Introduction

Thioether, such as dimethyl sulfide (CH_3SCH_3, DMS), methyl ethyl sulfide ($CH_3SCH_2CH_3$, MES), diethyl sulfide ($C_2H_5SC_2H_5$, DES), dipropyl sulfide ($C_3H_7SC_3H_7$, DPS) ,and dibutyl sulfide ($C_4H_9SC_4H_9$, DBS), are mainly emitted from the sea surface by biological activities [1, 2] and various industrial processes [3, 4]. These thioether compounds have been widely studied [5–10] because of their negative effects on the Earth's environment [11, 12].

MES is used in organic synthesis and fundamental scientific research [13, 14]. The reaction of thioether compound with OH radical is one of the most important degradation processes in the atmosphere [15]. Therefore, the reaction of MES with OH has been studied by several experiments. Hynes et al. [16] measured the hydrogen abstraction rate constant at 298 K in 40 Torr (Ar) was $(8.5 \pm 0.3) \times 10^{-12}$ cm^3 molecule^{-1} s^{-1} using conventional flash photolysis resonance fluorescence technique. They postulated the following mechanism (Scheme 1), and R2 was estimated to be dominant.

Scheme 1 Hynes et al. [16] postulated hydrogen abstraction channels

Besides, Williams et al. [17] measured the hydrogen abstraction rate constant at 245.2 K in 100 Torr (N_2) was $(1.35 \pm 1.69) \times 10^{-11}$ cm^3 molecule^{-1} s^{-1} using pulsed laser photolysis-pulsed fluorescence technique. Meanwhile, they found that the hydrogen abstraction rate constant of the title reaction at low sulfide concentrations without oxygen was independent of temperature and pressure, while adduct formation displayed dependence on the pressure. Recently, Gabriela et al. [18] determined the rate constant at 298 K and 1 atm was $(1.11 \pm 0.29) \times 10^{-11}$ cm^3 molecule^{-1} s^{-1} using long path in situ FTIR analysis. The result indicates that the most favorable hydrogen abstraction channel is abstract hydrogen atom from CH_2 group of $CH_3SCH_2CH_3$ by OH radical. To the best of our knowledge, no theoretical mechanism has been investigated for the title reaction until now. Moreover, enthalpies of formation of sulfur-containing species play an important role in modeling atmosphere sulfur cycle, whereas little information is available for enthalpies of formation of such species [19–26], which restricts the further research about these compounds.

In this paper, the reaction mechanism of MES with OH radical is studied. Then, based on the obtained mechanism information, rate constants are calculated using the conventional transition state theory (TST) including the Wigner tunneling correction and Rice-Ramsperger-Kassel-Marcus (RRKM) theory. Besides, enthalpies of formation of the species ($CH_2SCH_2CH_3$, CH_3SCHCH_3, $CH_3SCH_2CH_2$, CH_3CH_2SOH, $CH_3SOCH_2CH_3$, $CH_2SOCH_2CH_3$, and $CH_3SOCHCH_3$) are predicted.

2 Computational method

Equilibrium geometries and frequencies of all the species (reactants, transition states, complexes and products) were calculated using second-order Møller-Plesset perturbation theory (MP2) [27, 28] method with the 6-31+G(2d,p) basis set. All the species were identified for minima (number of imaginary frequencies, NIMAG = 0) or transition state (NIMAG = 1). Intrinsic reaction coordinate (IRC) calculations [29] were carried out at the MP2/6-31+G(2d,p) level of theory to ensure that each transition state connected the desired reactants and products along the reaction paths. Besides, zero-point energies (ZPE) of all the species were also calculated at the same level of theory. In order to obtain more reliable energies of each species on the potential energy profile, single-point energies were computed by the CCSD(T)/6-311+G(3df,p) method [30]. Unless otherwise specified, the CCSD(T)/6-311+G(3df,p) single-point energies with zero-point energy (ZPE) correction are used in the following discussions.

Enthalpies formation [$\Delta_f H^o_{(298.15K)}$] of the reactants and products were calculated by the atomization energy method at the CBS-QB3 [31, 32], G3 [33], and G3MP2 [34] levels of theory, respectively. For molecule M, the enthalpies of formation [$\Delta_f H^o_{(g,M,298.15K)}$] were given by Eq. (1) [19, 35],

$$\Delta_f H^o_{(g,M,298.15K)} = \sum_{atoms} \Delta_f H^o_{(g,298.15K)} - \sum_{atoms} D^o_{(g,298.15K)} \quad (1)$$

In Eq. (1), the atomization energy $\left[\sum_{atoms} D^o_{(g,298.15K)} \right]$ was computed by the following Eq. (2).

$$\sum_{atoms} D^o_{(g,298.15K)} = \sum_{atoms} H^o_{(g,298.15K)} - H^o_{(g,298.15K)}(M) \quad (2)$$

Where $\sum_{atoms} \Delta_f H^o_{(g,298.15K)}$ denotes experimental enthalpies of formation for the corresponding atoms, with reference [21] enthalpies of formation 52.10, 171.29, 59.56, and 66.25 kcal mol^{-1} for H, C, O and S atom, respectively, $\sum_{atoms} H^o_{(g,298.15K)}$ stands for the calculated enthalpies for the individual atoms, $H^o_{(g,298.15K)}(M)$ was the calculated enthalpy of the molecule M. All of the calculations were carried out using the Gaussian 03 program [36].

Rate constants for the title reaction over the temperature range of 200–900 K and 1 atm were computed using conventional transition state theory (TST) with the Wigner tunneling correction implemented in VKLab version 1.0 program [37, 38]. To describe the association process of the barrierless reaction $CH_3SCH_2CH_3 + OH \rightarrow RC$ [HO···S(CH_3)CH_2CH_3], the Morse potential function $E(R) = De\{1-exp[-\beta(R-Re)]\}^2$ was used to calculate the minimum energy path. Detailed calculations of Morse potential function can be found in supporting information [39]. Besides, the rate constant from 0.01 to 10 atm of a unimolecular step RC $\rightarrow$ TS1a $\rightarrow$ P1($CH_2SCH_2CH_3 + H_2O$) was also calculated with Rice-Ramsperger-Kassel-Marcus (RRKM) [40] theory implemented in the Chemrate program (version 1.5.8) [41]. The energetic and molecular parameters (molecular mass, moments of inertia, enthalpies of formation, vibrational frequencies, Lennard-Jones sigma, Lennard-Jones sigma epsilon) were used in the rate constant calculation. Computational details of RRKM and TST rate constant were shown in the supporting information. Further details of the complete treatment have been described elsewhere [42].

3 Results and discussion

The relative energies (E_R) to the reactants (MES + OH), zero-point energies (ZPE), electronic structure energies (E), total energies (E_T) and the values $<S^2>$ of all the species, and imaginary frequencies (v) of transition states

Table 1 The zero-point energies (ZPE), electronic energies (E), total energies (E_T), relative energies (E_R) to the reactants ($CH_3SCH_2CH_3 + OH$) (in kcal mol^{-1}) and the $<S^2>$ after spin annihilation of all the species, imaginary frequencies (v, cm^{-1}) of transition states

Species	ZPE[a]	E[b]	E_T^c	E_R	v[a]	$<S^2>$[a]
R (MES + OH)	72.30	−371,646.87	−371,574.57	0.00		0, 0
RC	75.26	−371,656.79	−371,581.53	−6.95		0.750
iso-RC	74.72	−371,651.26	−371,576.54	−1.95		0.750
TS1a	70.85	−371,645.75	−371,574.90	−0.33	1,660𝑖	0.750
TS1b	70.67	−371,645.53	−371,574.86	−0.29	1,449𝑖	0.750
TS1c	70.48	−371,641.68	−371,571.20	3.38	1,923𝑖	0.750
TS2a	70.88	−371,647.12	−371,576.24	−1.66	1,382𝑖	0.750
TS2b	70.76	−371,646.77	−371,576.01	−1.44	1,096𝑖	0.750
TS3a	70.89	−371,643.67	−371,572.78	1.80	1,903𝑖	0.750
TS3b	70.29	−371,641.15	−371,570.86	3.72	1,734𝑖	0.750
TS3c	70.37	−371,641.59	−371,571.22	3.35	1,610𝑖	0.750
TS4	73.58	−371,609.19	−371,535.61	38.96	1,587𝑖	0.753
TS5	73.61	−371,633.09	−371,559.48	15.10	556𝑖	0.751
TS6	73.66	−371,633.08	−371,559.42	15.16	584𝑖	0.751
TS7	69.80	−371,613.90	−371,544.10	30.81	1,980𝑖	0.750
TS8	68.49	−371,591.33	−371,522.84	51.73	1449𝑖	0.750
TS9	68.49	−371,590.93	−371,522.44	52.14	1,670𝑖	0.750
PC1	73.04	−371,674.31	−371,601.27	−26.70		0.750
PC2	73.11	−371,675.66	−371,602.55	−27.98		0.750
PC3ab	72.66	−371,667.74	−371,595.08	−20.50		0.750
PC3c	72.23	−371,664.67	−371,592.44	−17.87		0.750
PC5	71.36	−371,645.30	−371,573.94	0.63		0.750
PC6	72.02	−371,645.73	−371,573.71	0.86		0.750
P1 ($CH_2SCH_2CH_3 + H_2O$)	71.41	−371,669.63	−371,598.22	−23.65		0.750, 0
P2 ($CH_3SCHCH_3 + H_2O$)	71.55	−371,670.84	−371,599.29	−24.71		0.750, 0
P3 ($CH_3SCH_2CH_2 + H_2O$)	71.11	−371,662.03	−371,590.92	−16.35		0.750, 0
P4 ($CH_2SCH_3 + CH_3OH$)	72.40	−371,655.76	−371,583.36	−8.79		0.750, 0
P5 ($CH_3 + CH_3CH_2SOH$)	70.65	−371,643.41	−371,572.76	1.82		0.750, 0
P6 ($CH_3CH_2 + CH_3SOH$)	71.38	−371,643.16	−371,571.78	2.79		0.750, 0
P7 [$CH_3S(O)CH_2CH_3 + H$]	69.02	−371,626.71	−371,557.69	16.88		0.750, 0
P8 [$CH_2S(O)CH_2CH_3 + H_2$]	66.44	−371,625.98	−371,559.54	15.03		0.750, 0
P9 [$CH_3S(O)CHCH_3 + H_2$]	66.66	−371,629.10	−371,562.44	12.14		0.750, 0

[a] At the MP2/6-31+G(2d,p) level of theory

[b] At the CCSD(T)/6-311+G(3df,p) level of theory

[c] At the CCSD(T)/6-311+G(3df,p)//MP2/6-31+G(2d,p)+ZPE level of theory

are given in Table 1. As illustrated in Table 1, after spin annihilation for the doublet species, the value of $<S^2>$ is nearly 0.750 at the MP2/6-31+G(2d,p) level of theory, so the spin contamination is not severe. All optimized geometries of the reactants, complexes, transition states, and products at the MP2/6-31+G(2d,p) level of theory along with the available experimental values [43–47] are displayed in Fig. S1 and S2 in the supporting information. Similar calculations have validated that the MP2/6-31+G(2d,p) method is in good agreement with experimental geometries for the sulfur-containing species [17, 48]. Besides, previous investigations of the kinetics

and mechanism of organics reactions with a number of oxidants have shown that CCSD(T) method single-point energy results are reliable compared with the experimental values [49–51]. Potential energy profile for the reaction of $CH_3SCH_2CH_3$ with OH at the CCSD(T)/6-311+G(3df,p)//MP2/6-31+G(2d,p)+ZPE level of theory along with the transition states structures were shown in Figs. 1 and 2. The classical potential energy (V_{MEP}), the vibrationally adiabatic ground-state potential energy ($V_a^G = V_{MEP} + ZPE$), and the zero-point energy (ZPE) curve as a function of reaction coordinate s [(amu)$^{1/2}$ bohr] at the CCSD(T)/6-311+G(2d,p)//MP2/6-31+G(2d,p) level for Path R1a, R2a,

and R3a are depicted in Fig. S3. It can be seen in Fig. S3 that Path R1a has a low barrier height and smooth potential energy in the reaction region. The function of s from -1.5 to 1.5 [(amu)$^{1/2}$ bohr] is the reaction region for Path R1a. For the species (CH$_3$SCH$_2$CH$_3$, OH, H$_2$, CH$_3$OH, H$_2$O, CH$_3$), the mean absolute deviations of bond lengths and bond angles between the values at the MP2/6-31+G(2d,p) level of theory and the corresponding experiment ones are 0.004 Å and 0.71°, respectively. So the bond lengths and angles at the MP2/6-31+G(2d,p) level of theory are acceptable.

3.1 Reaction mechanism

Three hydrogen abstraction channels (R1–R3), one substitution process (R4) and five addition–elimination channels (R5–R9) are modeled for the title reaction, which are listed in Scheme 2, 3, where "RC" and "PC" denote post-reactant complex and pre-product complex of the corresponding reaction pathway, respectively.

3.1.1 Hydrogen abstraction mechanism

Eight transition state (TS) structures were located for the hydrogen abstraction of CH$_3$SCH$_2$CH$_3$ by OH radical. Three kinds of TS have been identified for H-abstraction from the α-CH$_3$ site (α-position carbon atom adjacent to the sulfur atom), α-CH$_2$ site, and β-CH$_3$ site (β-carbon atom stands away from the sulfur atom, see Fig. 1), respectively. Moreover, each hydrogen abstraction reaction channel can proceed in more than one way (pathway of reaction) due to the position of the abstracted hydrogen and sulfur atom of CH$_3$SCH$_2$CH$_3$ [52].

As described in Fig. 1, Fig. S1, and Scheme 2, in all the hydrogen abstraction transition states (TS1a, TS1b, TS1c, TS2a, TS2b, TS3a, TS3b, and TS3c), the breaking C–H bonds are elongated ranging from 6.2% (TS2b) to 9.3% (TS1c) compared with the equilibrium C–H bond in MES, whereas the forming O–H bonds are shorten ranging from 37% (TS3a) to 49% (TS2b) with respect to the O–H bond in H$_2$O. So the geometries of these transition states are reactant like, and have the characteristic of early transition states. Besides, the reaction energies of channel R1, R2, and R3 are -23.65, -24.71, and -16.35 kcal mol^{-1} at the CCSD(T)/6-311+G(3df,p)//MP2/6-31+G(2d,p) level of theory, respectively, which is in line with the Hammond's postulate [53].
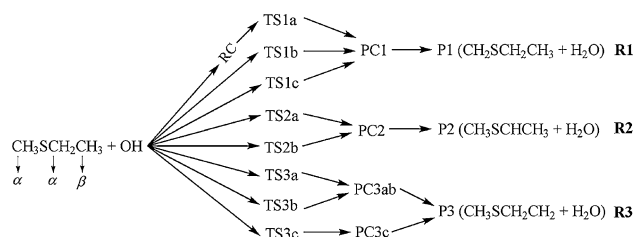
For channel R1, products P1 (CH$_2$SCH$_2$CH$_3$ + H$_2$O) are generated via transition state TS1a, TS1b and TS1c, which are labeled as Path R1a, R1b, and R1c, respectively. Path R1a begins with the formation of pre-reactant complex RC, while R1b and R1c are the direct hydrogen abstraction. The difference of these transition states is spatial orientation of the OH radical. Moreover, the barriers heights of path R1a (-0.33 kcal mol^{-1}) and R1b

(-0.29 kcal mol^{-1}) are lower than that of R1c (3.38 kcal mol^{-1}) (see Table 1), so path R1a and R1b are favorable.

For channel R2, products P2 (CH$_3$SCHCH$_3$ + H$_2$O) can be obtained directly via TS2a and TS2b, which are labeled as Path R2a and R2b, respectively. The major difference between TS2a and TS2b lies in dihedral angle $\angle$H(9)OH(4)C(2) (see Fig. 1). Hydrogen atom of the OH radical is directed toward the sulfur atom in TS2a ($\angle$H(9)OH(4)C(2) $= -7.91°$), whereas it is stays away from the sulfur atom in TS2b ($\angle$H(9)OH(4)C(2) $= 1.28°$) [8]. The imaginary frequencies of TS2a and TS2b are 1382$\imath$ cm^{-1} and 1096$\imath$ cm^{-1}, respectively. Channel R2 is easily to occur because of the low barrier heights (TS2a, -1.66 kcal mol^{-1}. TS2b, -1.44 kcal mol^{-1}).
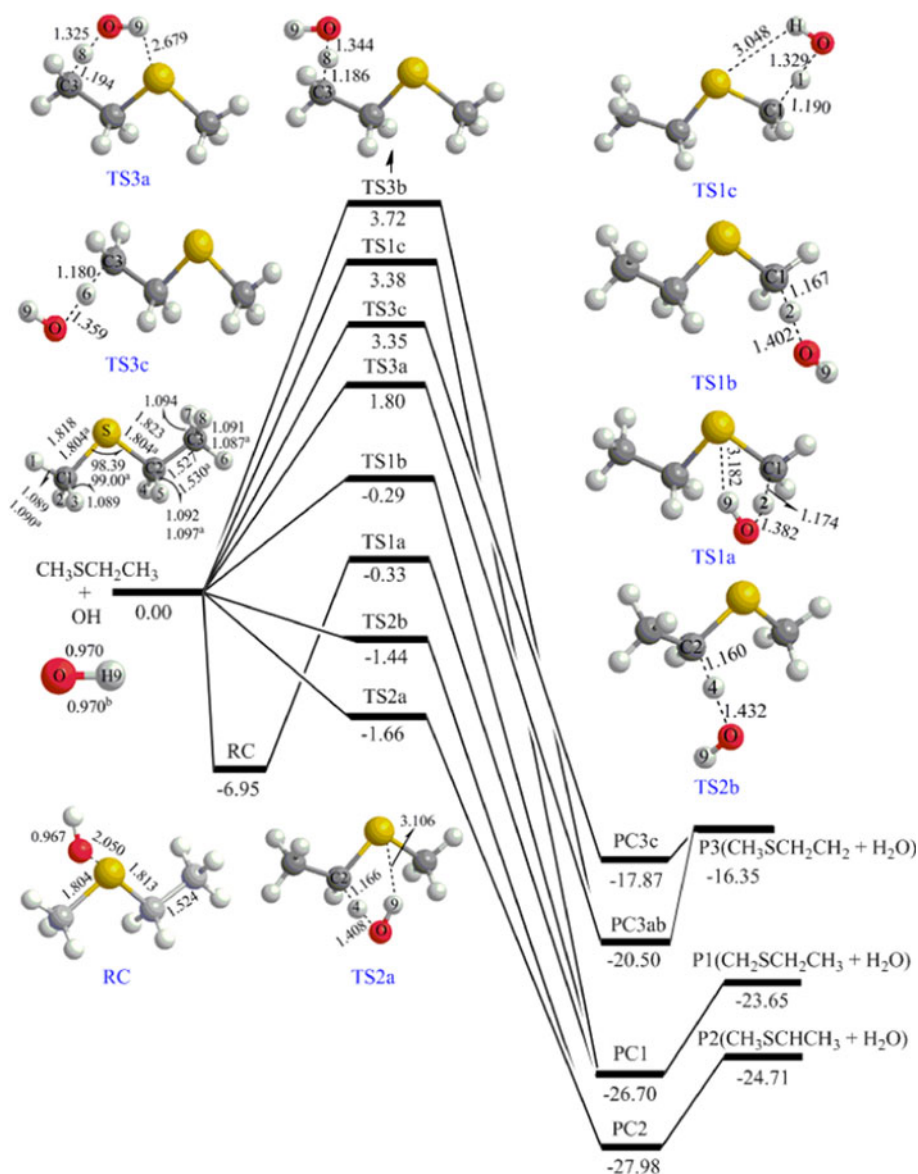
Channel R3 is proceeded via hydrogen abstraction from β-CH$_3$ by the O atom of OH radical. Three pathways, including Path R3a, R3b, and R3c, respectively via transition state TS3a, TS3b, and TS3c, have been identified. The barrier heights of Path R3a, R3b, and R3c are 1.80, 3.72, and 3.35 kcal mol^{-1}, respectively. This is probably because the interaction between H atom of the OH and S atom of the CH$_3$SCH$_2$CH$_3$ in TS3a (S···H, 2.679 Å) makes Path R3a easily take place, while such the interaction is not observed in TS3b and TS3c (see Fig. 1). The confirmation of the aforementioned interaction is based on the S···H bond length in the p-Cresol·H$_2$S complex (S···H, 2.437 Å) reported by Himansu et al. [54].

As discussed above, the hydrogen abstraction reactivity of CH$_3$SCH$_2$CH$_3$ by OH radical is found to decrease in the order of R2(α-CH$_2$ site) > R1(α-CH$_3$ site) > R3(β-CH$_3$ site) excluding Path R1c (see Scheme 2). The reactivity trend may be attributed to the atomic charges of C atom in CH$_3$SCH$_2$CH$_3$ [55, 56]. The Mulliken atomic charge of C atom of α-CH$_2$ in CH$_3$SCH$_2$CH$_3$ is 0.1733e, while Mulliken atomic charge of C atoms of α-CH$_3$ and β-CH$_3$ in CH$_3$SCH$_2$CH$_3$ are 0.0671e and -0.0849e, respectively. It can be easily understood that the more electropositive Mulliken atomic charge of C atom in CH$_3$SCH$_2$CH$_3$ is, the weaker the C–H bond of alkyl site in the CH$_3$SCH$_2$CH$_3$ becomes. Another interpretation of the hydrogen abstraction reactivity trend relies on the stability of the product radical. The stability order of the product radicals,
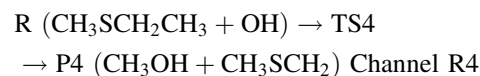

Scheme 2 Hydrogen abstraction pathways for the reaction CH$_3$SCH$_2$CH$_3$ + OH

Fig. 1 Schematic potential energy profiles of hydrogen abstraction channels for the reaction $CH_3SCH_2CH_3 + OH$. Bond lengths are in angstroms and angles are in degrees at the MP2/6-31+G(2d,p) level of theory along with the available experiment value [a], [b] are from references [43, 44], respectively. The relative energies to the reactants ($CH_3SCH_2CH_3 + OH$) were calculated at the CCSD(T)/6-311+G(3df,p)//MP2/6-31+G(2d,p) level of theory (in kcal mol^{-1})

CH_3SCHCH_3 (produced by R2) > $CH_2SCH_2CH_3$ (produced by R1) > $CH_3SCH_2CH_2$ (produced by R3), is in consistent with the hydrogen abstraction reactivity.

3.1.2 Substitution mechanism

R ($CH_3SCH_2CH_3 + OH$) → TS4
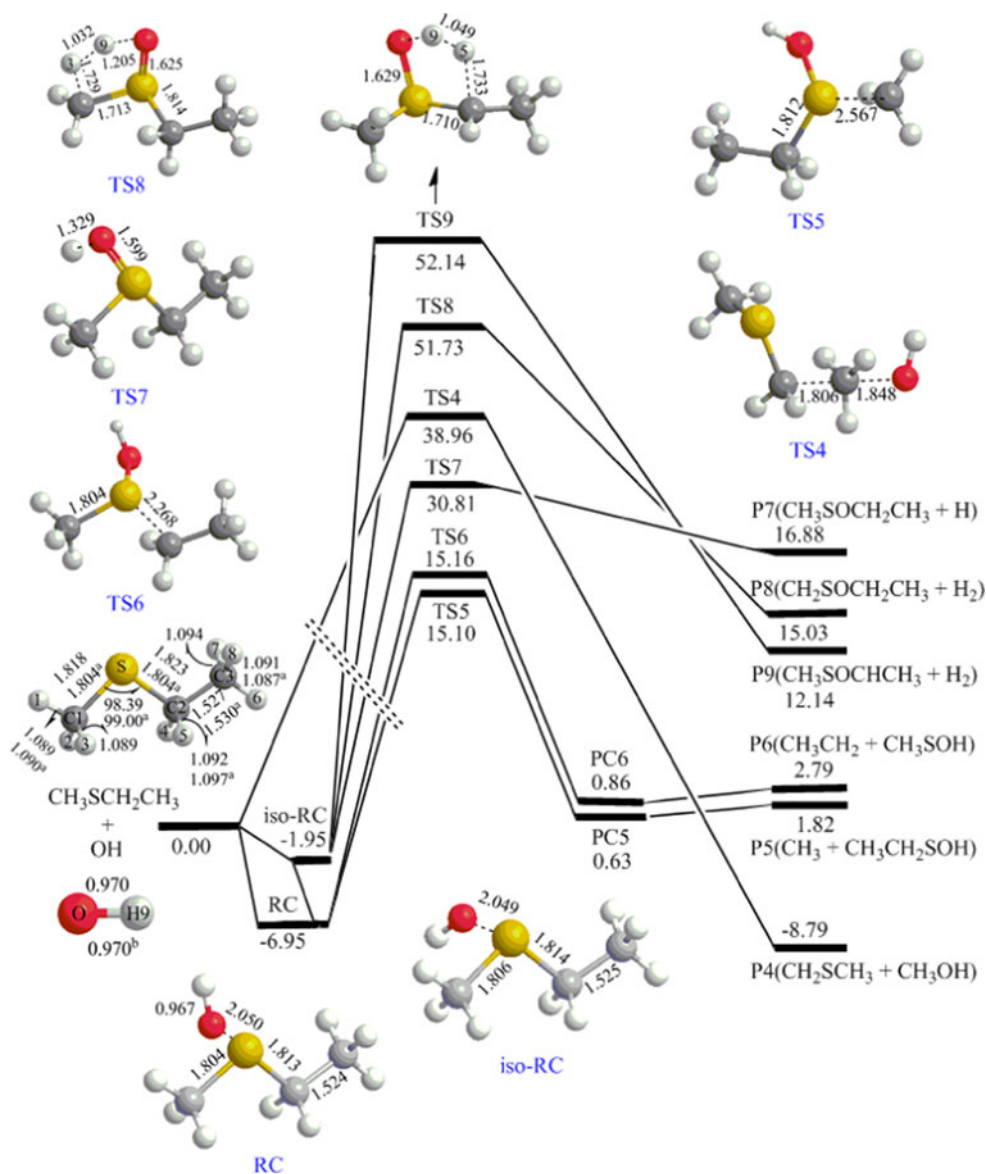 → P4 ($CH_3OH + CH_3SCH_2$) Channel R4

Channel R4 proceeded by the oxygen atom of OH radical attacking to the carbon atom of β-CH_3 and simultaneously C(2)–C(3) bond breaking. The corresponding transition state is TS4. In TS4, the breaking C(2)–C(3) bond is elongated by 0.279 Å compared with that in MES, while

the forming O–C(3) bond is 0.419 Å shorter than that in CH_3OH. The barrier height of R4 is 38.96 kcal mol^{-1}. Compared with the hydrogen abstraction channel, the substitution channel is kinetically unfeasible.

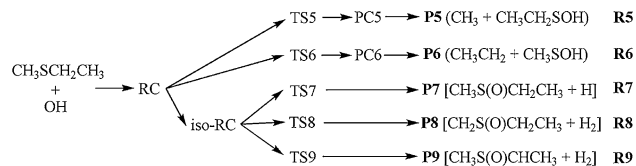### 3.1.3 Addition–elimination mechanism

All the addition–elimination channels (R5–R9) begin with post-reactant complex (HO$\cdots$S(CH$_3$)CH$_2$CH$_3$, denoted as RC). In order to describe the formation process of RC, the Morse potential function is employed to calculate the minimum energy path (shown in Fig. S4). The three parameters of this Morse potential function are $R_e = 2.050$ Å, $\beta = 1.81$ Å^{-1} and $De = 9.19$ kcal mol^{-1}

Fig. 2 Schematic potential energy profiles of substitution process and addition–elimination channels for the reaction $CH_3SCH_2CH_3 + OH$. Bond lengths are in angstroms and angles are in degrees at the MP2/6-31+G(2d,p) level along with the available experiment value [a], [b] are from references [43, 44], respectively. The relative energies to the reactants ($CH_3SCH_2CH_3 + OH$) were calculated at the CCSD(T)/6-311+G(3df,p)//MP2/6-31+G(2d,p) level of theory (in kcal mol^{-1})

Scheme 3 Addition–elimination pathways for the reaction $CH_3SCH_2CH_3 + OH$

at the MP2/6-31+G(2d,p) level of theory. It can be seen in Fig. S4 that the formation RC is a barrierless process, and the structure of RC is loose with a separation of 2.050 Å between the O atom of OH and the S atom of $CH_3SCH_2CH_3$. The relative energies of RC to the reactants ($CH_3SCH_2CH_3 + OH$) are listed in Table S1 at the various levels. The result indicates that the CCSD(T) method with 6-311++G(d,p) basis set for the relative energy calculation of RC to the reactants is −1.95 kcal mol^{-1}. This well depth indicates that the complex RC is not located, whereas substantial evidence for complex formation has provided in experiment [17]. With 6-31+G(2d,p) basis set when using CCSD(T) method, the relative energies of RC to the reactants is −6.00 kcal mol^{-1}, which is in good agreement with the experiment [17]. Besides, the differences for CCSD(T) method with the change of basis sets from the 6-31+G(2d,p),

6-311+G(2df,p), 6-311+G(3df,p), 6-311+G(3df,2p) to 6-311+G(3df,2pd) are little. For example, the difference in relative energies of RC to the reactants by using CCSD(T) method between 6-31+G(2d,p) and 6-311+G(3df,p) basis set are only 0.95 kcal mol^{-1}. It is concluded that addition of extra d function has great effect on the energetic calculation of RC with CCSD(T) method. Similar conclusion has been obtained for the calculation of the other sulfur-

containing species [19, 57]. Taking into account the computational accuracy and cost, we choose the CCSD(T)//6-311+G(3df,p)//MP2/6-31+G(2d,p) method to calculate the single-point energies of all the species.

Channel R5 and R6 start with the RC, which lead to the formation of P5 (CH$_3$+CH$_3$CH$_2$SOH) and P6 (CH$_3$CH$_2$+CH$_3$SOH) via TS5 and TS6, respectively. The breaking C(1)-S bond is elongated from 1.804 Å in RC to 2.567 Å in TS5, and the breaking C(2)-S bond is elongated from 1.813 Å in RC to 2.268 Å in TS6. The barrier heights of R5 and R6 are 15.10 and 15.16 kcal mol^{-1}, respectively.

RC can also isomerize to the iso-RC. As illustrated in Fig. 2, Fig. S1, and Scheme 3, the major difference between RC and iso-RC is the orientation of OH radical. In spite of many attempts, no transition state is found for this isomerization. Then, iso-RC can undergo further dissociation, and channel R7–R9 are verified. Channel R7 is the H-elimination reaction via TS7. The breaking O–H bond in TS7 is 0.316 Å longer than the corresponding value in iso-RC. The barrier height of R7 is 30.81 kcal mol^{-1}. Channel R8 and R9 are H$_2$-elimination reactions via five-membered ring transition state TS8 and TS9, respectively. As illustrated in Fig. S1, for the structures of TS8 and TS9, the breaking C–H bond is elongated by 58 and 58%, whereas the forming H–H bond is shortened by 55 and 58%, respectively, compared with the corresponding bond length in iso-RC. The barrier heights of R8 and R9 are 51.73 and 52.14 kcal mol^{-1}, respectively (showed in Table 1).

Oxygen gas is relatively abundant in the atmosphere, which also plays an important in the atmosphere chemistry reaction process. We give the complex formed between RC [(HO···S(CH$_3$)CH$_2$CH$_3$] and ^{3}O$_2$ in Fig. S5 in the supporting information. The result indicates the relative energy of complex [(OO)···S(OH)(CH$_3$)CH$_2$CH$_3$] to sum energy of RC + ^{3}O$_2$ is −11.77 kcal mol^{-1} at the CCSD(T)//6-311+G(2d,p)//MP2/6-31+G(2d,p) level of theory, which is more stable than that of [(OO···HO)··· S(CH$_3$)CH$_2$CH$_3$] by 0.96 kcal mol^{-1}. In this article, we focus on the reaction of CH$_3$SCH$_2$CH$_3$ with OH in the absence of ^{3}O$_2$, the further mechanism for the reaction of RC with ^{3}O$_2$ is not mentioned.

In summary, hydrogen abstraction is dominant. Substitution process and addition–elimination channels may be negligible due to the high barrier heights.

3.2 Enthalpies of formation of the reactants and products

Formation enthalpies [$\Delta_f H^O_{(g,M,298.15K)}$] of the reactants (CH$_3SCH_2CH_3$, OH) and products (CH$_2SCH_2CH_3$, CH$_3$SCHCH$_3$, CH$_3SCH_2CH_2$, H$_2O, CH_3OH, CH_3SCH_2$, CH$_3$, CH$_3CH_2$, CH$_3CH_2SOH, CH_3$SOCH$_2CH_3$, CH$_2$SOCH$_2CH_3$

and CH$_3$SOCHCH$_3$) are calculated by the atomization energy method [35]. The CBS-QB3, G3, and G3MP2 are selected to evaluate the enthalpy of formation because these methods can offer accurate calculation of formation enthalpy [58, 59]. As listed in Table 2, the calculated enthalpies of formation for the species (OH, H$_2$O, CH$_3$SCH$_2$, CH$_3$OH, CH$_3$, CH$_3$CH$_2$, H$_2$, and CH$_3$SCH$_2$ CH$_3$) by the aforementioned three methods are in accordance with the corresponding experiment values [21, 26]. For example, the maximum deviations between the calculated enthalpies of formation by the aforementioned three methods and the corresponding experimental ones are −1.13 (H$_2$), −0.98 (CH$_3$), and −1.14 kcal mol^{-1} (H$_2$), respectively. Besides, the mean absolute deviations between the enthalpies of formation by the aforementioned three methods and the corresponding experimental ones are 0.49, 0.41 and 0.50 kcal mol^{-1}, respectively. From the viewpoint of maximum deviation and mean absolute deviation, the enthalpies of formation by the G3 method are more reliable than that of CBS-QB3 and G3MP2. Enthalpies of formation of species CH$_2$SCH$_2$CH$_3$, CH$_3$SCHCH$_3$, CH$_3$SCH$_2$CH$_2$, CH$_3$CH$_2$SOH, CH$_3$SOCH$_2$CH$_3$, CH$_2$SO CH$_2$CH$_3$ and CH$_3$SOCHCH$_3$ at the G3 level of theory are 27.77, 26.83, 35.20, −39.05, −40.45, 9.09 and 6.44 kcal mol^{-1}, respectively. These results can be used for the atmosphere sulfur cycle modeling application.

3.3 Rate constant calculation

The TST and RRKM rate constant calculations of the selected channel were shown in Scheme 4, where "RC", "PC" and "k" denote post-reactant complex, pre-product complex and rate constant of the corresponding reaction pathway, respectively. We neglect the rate constant calculation of channel R4 and R7-R9 because of their high barriers. The energies, vibrational frequencies, and moments of inertia used in the rate constant calculation are listed in Table 1 and Table S2.

In the TST calculation, the total rate constant k_{total} are calculated within the temperature range of 200–900 K and 1 atm, which was given by

$$k_{total} = K_{eq} \cdot k_{1a-1} + k_{1b} + k_{1c} + k_{2a} + k_{2b} + k_{3a} + k_{3b} + k_{3c} + K_{eq} \cdot k_{5-1} + K_{eq} \cdot k_{6-1}$$

As listed in Fig. 3 and Table S3, the value of k_{total} at 298 K is 1.68×10^{-11} cm^3 molecule^{-1} s^{-1}, which is close to the experimental value $(8.5 \pm 0.3) \times 10^{-12}$ [16] and $(1.11 \pm 0.29) \times 10^{-11}$ [18] cm^3 molecule^{-1} s^{-1}. As the temperature increases, k_{total} decreases slowly in the temperature range of 200–450 K ($k_{total}^{450}/k_{total}^{200} = 0.31$), and increases within the temperature range of 450–900 K ($k_{total}^{900}/k_{total}^{450} = 2.12$). The results over the temperature range

Table 2 The calculated enthalpies of formation [$\Delta_f H^o_{(g,298.15K)}$] (in kcal mol^{-1}) using CBS-QB3, G3 and G3MP2 methods along with the available experimental values
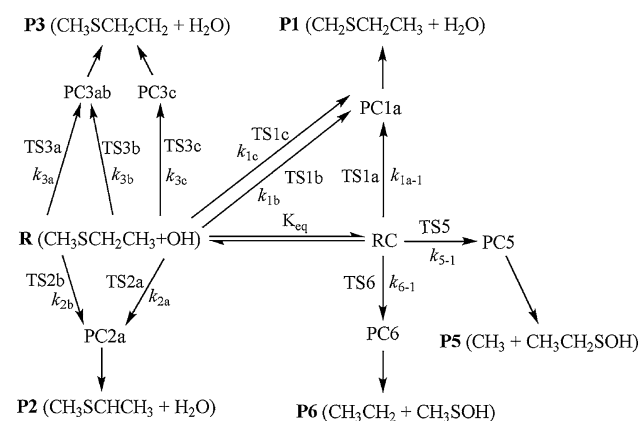
Species	$\Delta_f H^o_{(g,298.15K)}$			
	CBS-QB3	G3	G3MP2	Exp
OH	8.95 (0.04)	8.54 (−0.37)	8.44 (−0.47)	8.91[a]
H$_2$O	−58.08 (−0.29)	−57.34 (0.45)	−57.28 (0.51)	−57.79[a]
CH$_3$SCH$_2$	32.73 (0.03)	33.32 (0.62)	32.80 (0.10)	32.70[a]
CH$_3$OH	−48.68 (−0.64)	−47.93 (0.11)	−47.46 (0.58)	−48.04[a]
CH$_3$	35.55 (0.50)	34.07 (−0.98)	34.27 (−0.78)	35.05[a]
CH$_3$CH$_2$	29.97 (1.07)	28.82 (−0.08)	29.03 (0.13)	28.90[a]
H$_2$	−1.13 (−1.13)	−0.46 (−0.46)	−1.14 (−1.14)	0.00[a]
CH$_3$SCH$_2$CH$_3$	−14.65 (−0.29)	−14.10 (0.26)	−14.66 (−0.30)	−14.36[b]
MAD[c]	(0.49)	(0.41)	(0.50)	
CH$_2$SCH$_2$CH$_3$	27.59	27.77	27.32	
CH$_3$SCHCH$_3$	26.25	26.83	26.35	
CH$_3$SCH$_2$CH$_2$	35.18	35.20	34.58	
CH$_3$CH$_2$SOH	−40.58	−39.05	−39.05	
CH$_3$SOCH$_2$CH$_3$	−41.80	−40.45	−40.41	
CH$_2$SOCH$_2$CH$_3$	8.16	9.09	9.24	
CH$_3$SOCHCH$_3$	5.02	6.44	6.55	

In table, the values in the parentheses are the enthalpy of formation deviations between the calculated values and the corresponding experimental ones
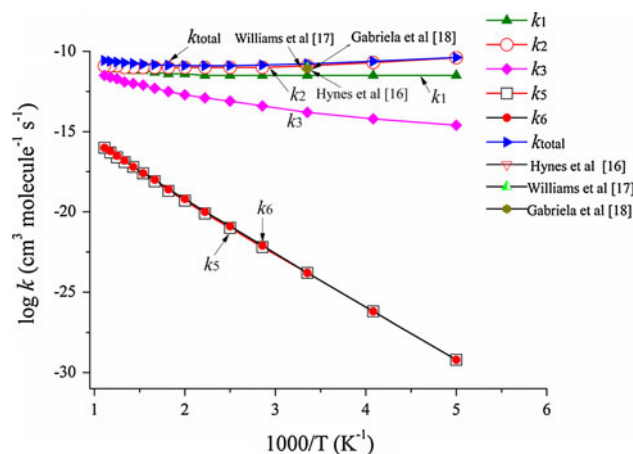
[a] From Ref. [21]

[b] From Ref. [26]

[c] Denotes mean absolute deviation

Scheme 4 The selected reaction channels in rate constant calculations

Fig. 3 Rate constants calculated in this work are plotted as a function of temperature (200–900 K) along with the available experiment values [16–18]. k_1 ($k_1 = k_{1a} + k_{1b} + k_{1c}$) is rate constant for channel R1. k_2 ($k_2 = k_{2a} + k_{2b}$) is rate constant of channel R2, k_3 ($k_3 = k_{3a} + k_{3a} + k_{3c}$) is rate constant of channel R3, k_{total} is the sum of k_1, k_2, k_3, k_5 and k_6. The k_{1a}, k_{1b}, k_{1c}, k_{2a}, k_{2b}, k_{3a}, k_{3b}, k_{3c}, k_5 and k_6 represent the rate constants of R1a, R1b, R1c, R2a, R2b, R3a, R3b, R3c, R5 and R6, respectively

of 240–295 K ($k_{total}^{295}/k_{total}^{240} = 0.70$) is in reasonable agreement with the experimental values ($k_{total}^{295}/k_{total}^{240} = 0.94$) reported by Williams et al. [17].

The branching ratios of channel R1, R2, R3, R5, and R6 are described in Fig. 4 and Table S4. It can be seen in Fig. 4 and Table S4 that the total rate constant in the temperature of 200–900 K and 1 atm are mainly depended

on the R1 and R2. The contribution of R2 to the total rate constant is always larger than R1 (k_1/k_{total}, 16.9%, k_2/k_{total}, 75.2%, 298.15 K). As the temperature increases, R1
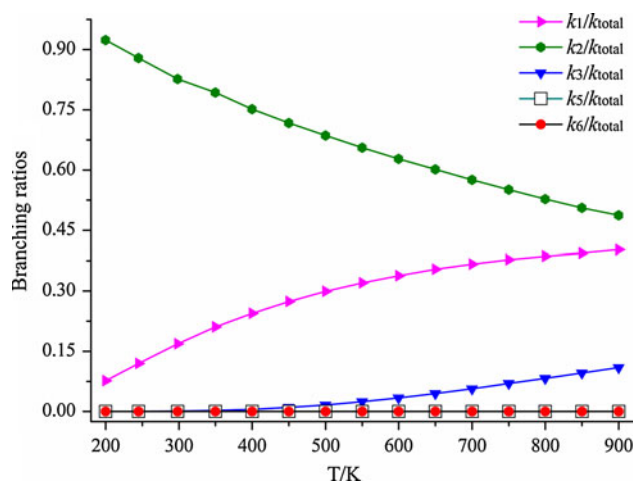
Fig. 4 The predicted branching ratios over the temperature range of 200–900 K. The k_1/k_{total}, k_2/k_{total}, k_3/k_{total}, k_5/k_{total} and k_6/k_{total} represent the branching ratios of channel R1, R2, R3, R5 and R6, respectively

becomes significant at 900 K (k_1/k_{total}, 40.2%, k_2/k_{total}, 48.7%, 900 K). The contribution of R3 to the total rate constant over the temperature of 200–900 K is small within 11%.

For kinetic modeling applications, the rate constant k_1, k_2, k_3, k_5, k_6, and k_{total} in the temperature range of 200–900 K have been fitted to the three-parameter expressions (unit in cm^3 molecule^{-1} s^{-1}):

$$k_1 = 1.15 \times 10^{-20} T^{2.89} \exp(-826.24/T)$$

$$k_2 = 6.36 \times 10^{-20} T^{2.60} \exp(-1306.78/T)$$

$$k_3 = 8.50 \times 10^{-25} T^{4.28} \exp(179.35/T)$$

$$k_5 = 2.72 \times 10^{-20} T^{2.31} \exp(6874.51/T)$$

$$k_6 = 1.37 \times 10^{-19} T^{2.12} \exp(7001.67/T)$$

$$k_{total} = 1.45 \times 10^{-21} T^{3.24} \exp(-1384.54/T)$$

In order to describe the pressure effect qualitatively, the RRKM rate constant [60] for a unimolecular reaction step RC[HO⋯S(CH$_3$)CH$_2$CH$_3$] → TS1a → P1(CH$_2$SCH$_2$CH$_3$ + H$_2$O) from 0.01 to 10 atm and 300 K was carried out with chemrate program. Collisional energy transfer was described using an exponential down model with $<\Delta E_{down}>$=200 cm^{-1}. Lennard-Jone collision parameters [61] for the intermediate RC are $\sigma = 4.94$ Å and $\varepsilon = 602.5$ K, which are approximately the same as those of CH$_3$SOCH$_3$. N$_2$, $\sigma = 3.74$ Å and $\varepsilon = 82$ K, are used as the buffer gas. Fall off curve of the reaction RC → TS1a → P1(CH$_2$SCH$_2$CH$_3$ + H$_2$O) as a function of pressure (0.01–10 atm) at 300 K are shown in Fig. S6. As described in Fig. S6, the rate constant increases rapidly in the pressure range of 0.01–1.42 atm, whereas it rises very slowly within the pressure range of 1.42–10 atm.

4 Conclusions

Theoretical method CCSD(T)/6-311+G(3df,p)//MP2/6-31+G(2d,p) is applied to study the reaction mechanism of CH$_3$SCH$_2$CH$_3$ with OH. Enthalpies of formation of the reactants and products are predicted at the CBS-QB3, G3, and G3MP2 levels of theory, respectively. The TST rate constants with the Wigner tunneling correction are evaluated over the temperature range of 200–900 K. The main conclusions are summarized as follows:

(1) Three possible channels are investigated for the reaction of CH$_3$SCH$_2$CH$_3$ + OH, namely, hydrogen abstraction, addition–elimination, and substitution. The results indicate that hydrogen abstraction is more favorable than addition–elimination and substitution.

(2) The rate constants are evaluated over the temperature range of 200–900 K. The contribution of hydrogen abstraction from α-CH$_2$ to the total rate constant is greater than that of hydrogen abstraction from α-CH$_3$ over the temperature of 200–900 K, whereas the competition of hydrogen abstraction from α-CH$_3$ and hydrogen abstraction from α-CH$_2$ becomes obvious competitive with the temperature increases to 900 K.

(3) Enthalpies of formation of the reactants and products are predicted at the CBS-QB3, G3, and G3MP2 levels of theory, respectively. The enthalpies of formation by G3 method are more accurate than that of CBS-QB3 and G3MP2 in terms of maximum deviation and mean absolute deviation. The predicted enthalpies of formation of species CH$_2$SCH$_2$CH$_3$, CH$_3$SCHCH$_3$, CH$_3$SCH$_2$CH$_2$, CH$_3$CH$_2$SOH, CH$_3$SOCH$_2$CH$_3$, CH$_2$SOCH$_2$CH$_3$, and CH$_3$SOCHCH$_3$ at the G3 level of theory are 27.77, 26.83, 35.20, −39.05, −40.45, 9.09, and 6.44 kcal mol^{-1}.

References

1. Bentley R, Chasteen TG (2004) Chemosphere 55:291
2. Buzzini P, Romano S, Turchetti B, Vaughan A, Pagnoni UM, Davoli P (2005) FEMS Yeast Res 5:379
3. Smet E, Van Langenhove H (1998) Biodegradation 9:273
4. Torén K, Hagberg S, Westberg H (1996) Am J Ind Med 29:111
5. Aloisio S (2006) Chem Phys 326:335
6. Gonzalez Garcia N, Gonzalez Lafont A, Lluch JM (2005) J Comput Chem 26:569
7. Wang K, Du L, Ge M (2009) J Environ Sci (China) 21:137

8. El-Nahas AM, Uchimaru T, Sugie M, Tokuhashi K, Sekiya A (2005) J Mol Struct Theochem 722:9

9. Williams MB, Campuzano Jost P, Hynes AJ, Pounds AJ (2009) J Phys Chem A 113:6697

10. Jee J, Tao FM (2006) J Phys Chem A 110:7682

11. Chasteen TG, Bentley R (2004) J Chem Educ 81:1524

12. Lomans BP, Van der Drift C, Pol A, Op den Camp HM (2002) CMLS Cell Mol Life Sci 59:575

13. Domine F, Murrells TP, Howard CJ (1990) J Phys Chem 94:5839

14. Domine F, Ravishankara AR, Howard CJ (1992) J Phys Chem 96:2171

15. Barnes I, Hjorth J, Mihalopoulos N (2006) Chem Rev 106:940

16. Hynes AJ, Wine PH, Semmes DH (1986) J Phys Chem 90:4148

17. Williams MB, Campuzano Jost P, Pounds AJ, Hynes AJ (2007) Phys Chem Chem Phys 9:4370

18. Oksdath-Mansilla G, Peñéñory AB, Albu M, Barnes I, Wiesen P, Teruel MA (2009) Chem Phys Lett 477:22

19. Vandeputte A, Reyniers M-F, Marin G (2009) Theor Chem Acc 123:391

20. Atkinson R, Baulch DL, Cox RA, Crowley JN, Hampson RF, Hynes RG, Jenkin ME, Rossi MJ, Troe J (2004) Atmos. Chem Phys 4:1461

21. Sander SP, Friedl RR, Golden DM, Kurylo MJ, Moortgat GK, Keller-Rudek H, Wine PH, Ravishankara AR, Kolb CE, Molina MJ, Finlayson-Pitts BJ, Huie RE, Orkin VL (2006) Chemical kinetics and photochemical data for use in atmospheric studies, evaluation number 15, California National Aeronautics and Space Administration, Jet Propulsion Laboratory, Pasadena. http://jpldataevaljplnasagov/. Accessed 20 Jan 2011

22. Resende SM, Ornellas FR (2003) Chem Phys Lett 367:489

23. Grant DJ, Dixon DA, Francisco JS, Feller D, Peterson KA (2009) J Phys Chem A 113:11343

24. Szori M, Csizmadia IG, Fittschen C, Viskolcz B (2009) J Phys Chem A 113:9981

25. Wheeler SE, Schaefer HF (2009) J Phys Chem A 113:6779

26. NIST Chemistry Webbook. http://webbook.nist.gov/chemistry. Accessed 20 Jan 2011

27. Møller C, Plesset MS (1934) Phys Rev 46:618

28. Head-Gordon M, Pople JA, Frisch MJ (1988) Chem Phys Lett 153:503

29. Gonzalez C, Schlegel HB (1989) J Chem Phys 90:2154

30. Raghavachari K, Trucks GW, Pople JA, Head-Gordon M (1989) Chem Phys Lett 157:479

31. Petersson GA, Bennett A, Tensfeldt TG, Al-Laham MA, Shirley WA, Mantzaris J (1988) J Phys Chem 89:2193

32. Montgomery JJA, Frisch MJ, Ochterski JW, Petersson GA (1999) J Chem Phys 110:2822

33. Curtiss LA, Raghavachari K, Redfern PC, Rassolov V, Pople JA (1998) J Chem Phys 109:7764

34. Curtiss LA, Redfern PC, Raghavachari K, Rassolov V, Pople JA (1999) J Chem Phys 110:4703

35. Curtiss LA, Raghavachari K, Redfern PC, Pople JA (1997) J Chem Phys 106:1063–1079

36. Frisch MJ et al (2004) Gaussian 03, revision C. 02. Gaussian Inc, Wallingford, CT

37. Duncan WT, Bell RL, Truong TN (1998) J Comput Chem 19(9):1039

38. Zhang SW, Truong TN (2001) VKLab version 1.0. University of Utah, Utah

39. Jian R-C, Tsai C, Hsu L-C, Chen H-L (2010) J Phys Chem A 114:4655

40. Barker JR, Golden DM (2003) Chem Rev 103:4577

41. Mokrushin V, Bedanov V, Tsang W, Zachariah M, Knyazev V (2009) ChemRate, version 1.5.8. National Institute of Standards and Testing, Gaithersburg, MD

42. Miller JA, Klippenstein SJ (2006) J Phys Chem A 110(36):10528

43. Kuchitsu K (ed) (1987) Landolt Bornstein: Group II: atomic and molecular physics, vol 15: structure data of free polyatomic molecules. Springer, Berlin

44. Huber KP, Herzberg G (1979) Van Nostrand Reinhold Co. http://cccbdb.nist.gov/exp1.asp. Accessed 20 Jan 2011

45. Venkateswarlu P, Gordy W (1955) J Chem Phys 23:1200

46. Hoy AR, Cavers PB (1979) J Mol Spectrosc 74:1

47. Herzberg G (1966) Van Nostrand, New York. http://cccbdb.nist.gov/exp1.asp. Accessed 20 Jan 2011

48. Bergès J, Varmenot N, Scemama A, Abedinzadeh Z, Bobrowski K (2008) J Phys Chem A 112:7015

49. Lei W, Zhang R, Sean McGivern W, Derecskei-Kovacs A, North SW (2000) Chem Phys Lett 326:109

50. Suh I, Lei W, Zhang R (2001) J Phys Chem A 105:6471

51. Zhang D, Zhang R, Park J, North SW (2002) J Am Chem Soc 124:9600

52. Zavala-Oseguera C, Alvarez-Idaboy JR, Merino G, Galano A (2009) J Phys Chem A 113:13913

53. Hammond GS (1955) J Am Chem Soc 77:334

54. Biswal HS, Shirhatti PR, Wategaonkar S (2009) J Phys Chem A 113:5633

55. Nam PC, Nguyen MT, Chandra AK (2005) J Phys Chem A 109:10342

56. Huynh LK, Ratkiewicz A, Truong TN (2006) J Phys Chem A 110:473

57. Zhu L, Bozzelli JW (2005) J Mol Struct Theochem 728:147

58. Montgomery JJA, Frisch MJ, Ochterski JW, Petersson GA (2000) J Chem Phys 112:6532

59. Denis PA (2004) J Phys Chem A 108:11092

60. Glowacki DR, Pilling MJ (2010) Chem Phys Chem 11:3836

61. Mourits FM, Rummens HA (1977) Can J Chem 55:3007